



Article

Multistep Photochemical Reactions of Polypyridine-Based Ruthenium Nitrosyl Complexes in Dimethylsulfoxide

Nataliia Marchenko ¹, Pascal G. Lacroix ^{1,*}, Valerii Bukhanko ¹, Marine Tassé ¹, Carine Duhayon ¹, Martial Boggio-Pasqua ^{2,*}  and Isabelle Malfant ^{1,*} 

¹ LCC (Laboratoire de Chimie de Coordination), CNRS, 205, route de Narbonne, F-31077 Toulouse, France; marchenko.nataliia01@gmail.com (N.M.); valerkabu@gmail.com (V.B.); marine.tasse@lcc-toulouse.fr (M.T.); carine.duhayon@lcc-toulouse.fr (C.D.)

² Laboratoire de Chimie et Physique Quantiques, Université Paul Sabatier (Toulouse), UMR 5626, 218 route de Narbonne, F-31077 Toulouse, France

* Correspondence: pascal.lacroix@lcc-toulouse.fr (P.G.L.); martial.boggio@irsamc.ups-tlse.fr (M.B.-P.); isabelle.malfant@lcc-toulouse.fr (I.M.); Tel.: +33-561333188 (P.G.L.)

Academic Editor: Derek J. McPhee

Received: 26 March 2020; Accepted: 3 May 2020; Published: 8 May 2020



Abstract: The photorelease of nitric oxide (NO·) has been investigated in dimethylsulfoxide (DMSO) on two compounds of formula [Ru(R-tpy)(bpy)(NO)](PF₆)₃, in which bpy stands for 2,2'-bipyridine and R-tpy for the 4'-R-2,2':6',2''-terpyridine with R = H and MeOPh. It is observed that both complexes are extremely sensitive to traces of water, leading to an equilibrium between [Ru(NO)] and [Ru(NO₂)]. The photoproducts of formula [Ru(R-tpy)(bpy)(DMSO)](PF₆)₂ are further subjected to a photoreaction leading to a reversible linkage isomerization between the stable Ru-DMSO_(S) (sulfur linked) and the metastable Ru-DMSO_(O) (oxygen linked) species. A set of 4 [Ru(R-tpy)(bpy)(DMSO)]²⁺ complexes (R = H, MeOPh, BrPh, NO₂Ph) is investigated to characterize the ratio and mechanism of the isomerization which is tentatively related to the difference in absorbance between the Ru-DMSO_(S) and Ru-DMSO_(O) forms. In addition, the X-ray crystal structures of [Ru(tpy)(bpy)(NO)](PF₆)₃ and [Ru(MeOPh-tpy)(bpy)(DMSO_(S))](PF₆)₂ are presented.

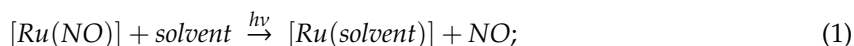
Keywords: nitric oxide; DFT computations; photochemistry; ruthenium complexes

1. Introduction

Nitric oxide (NO·) is a radical involved in numerous biological functions, such as blood pressure regulation, stimulation of immune response or neurotransmission, which has been observed to exhibit various anticancer, antibacterial, and anti-inflammatory activities [1]. For these reasons, intense research efforts have been directed towards the design of exogenous NO· donors capable of releasing NO· locally and quantitatively [2,3]. Among potential candidates, ruthenium-nitrosyl [Ru(NO)] complexes appear especially promising due to their usually low toxicity, good chemical stability and their capability to release NO· under irradiation in the $\lambda = 300\text{--}600$ nm domain, exclusively [4–13]. In practice, and to overpass the frequently modest solubility of metal-nitrosyl complexes in biological media, the complexes are generally dissolved in aqueous solutions containing a maximum in volume of 0.5% of dimethylsulfoxide (DMSO) before being tested on living cells. In this context, the stability and photochemical reactivity of [Ru(NO)] species in DMSO is naturally addressed. Indeed, DMSO is a potential ligand for ruthenium complexes [14]. Furthermore, several examples of [Ru(DMSO)] species have been found to be photo-isomerizable, which could also broaden the range of applications of these versatile species [15–20].

In a research effort aimed at checking out the full behavior of [Ru(NO)] complexes in DMSO environment, the chemical and photochemical properties of [Ru(MeOPh-tpy)(bpy)(NO)]³⁺

([RuT1B0(NO)]³⁺ in Figure 1), where MeOPh-tpy is the 4'-(4-methoxyphenyl)-2,2':6',2''-terpyridine, and bpy the 2,2'-bipyridine, have been investigated. [RuT1B0(NO)]³⁺ has been selected as a benchmark candidate for NO· release, due to its “push-pull” character between the electron-rich methoxyphenyl and the electron-withdrawing nitrosyl (NO) substituents. This effect has long been expected to enhance the charge transfer towards the nitrosyl and hence to favor the NO· release capabilities, according to the following overall reaction [5]:



Furthermore, the electronic “push-pull” character of [RuT1B0(NO)]³⁺ is expected to enhance the two-photon absorption (TPA) properties, which is highly desirable for practical applications in the $\lambda = 600\text{--}1200$ nm therapeutic window under two-photon irradiation, the method of choice for drugs photodelivery in biological media [21,22]. A reference complex of formula [Ru(tpy)(bpy)(NO)]³⁺ ([RuT0B0(NO)]³⁺ in Figure 1), will be presented in parallel to [RuT1B0(NO)]³⁺, to elucidate the NO· photorelease process in DMSO medium. In a last section, two additional complexes of formula [RuT2B0(DMSO)]³⁺ and [RuT3B0(DMSO)]³⁺, where T2 an T3 state for 4'-(4-(bromo)phenyl)-2,2':6',2''-terpyridine and 4'-(4-(nitro)phenyl)-2,2':6',2''-terpyridine, respectively, will be presented to fully investigate the possibilities for Ru-DMSO_(S) to Ru-DMSO_(O) linkage isomerizations (Figure 1).

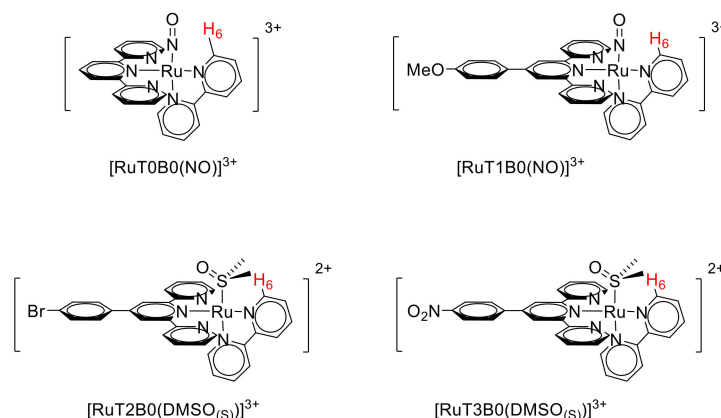


Figure 1. Ruthenium complexes under investigation. Proton H6 used for the NMR characterization is indicated in red color on the bipyridine ligand.

2. Results and Discussion

2.1. Photo-Chemical Behavior of [Ru(R-tpy)(bpy)(NO)]³⁺ in DMSO: the First Step

The ¹H-NMR monitoring of the continuous irradiation of [RuT1B0(NO)](PF₆)₃ in deuterated DMSO (DMSO-*d*₆) is shown in Figure 2a. ¹H-NMR appears to be an excellent tool for defining the coordination sphere of [Ru(tpy)(bpy)X] species. We have previously reported that the chemical shift of the proton in position 6 on the bipyridine, is very sensitive to the nature of the X ligand attached to the ruthenium center, due to the spatial proximity between H-6 and X and the subsequent different electronic environment (Figure 1) [23,24]. Three different compounds (A, B, C) are observed on the spectra, with various concentrations throughout the irradiation process. The integrations of the NMR signals allows drawing the relative concentrations in Figure 2b, where the sum of the concentrations [A] + [B] + [C] is normalized to 1, at any reaction time.

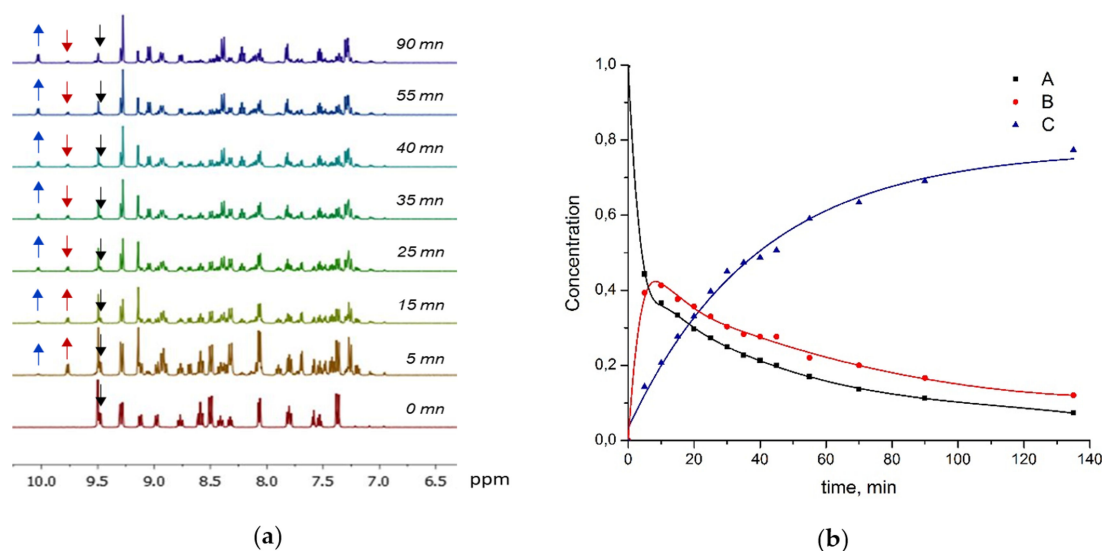
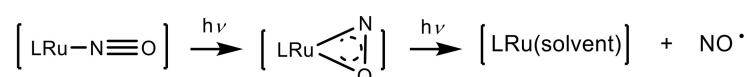


Figure 2. (a) $^1\text{H-NMR}$ tracking during the irradiation of $[\text{RuT1B0}(\text{NO})](\text{PF}_6)_3$ (A) in $\text{DMSO-}d_6$, at $\lambda = 395 \text{ nm}$ (black, red, blue arrows for A, B, C respectively). (b) Relative concentrations of A, B, and C, from the NMR integrated signals.

The examination of Figure 2 reveals that the starting compound (A) is gradually transformed to the final product (C), B appearing as a possible intermediate in a global photoreaction which, at first, can tentatively be written as $\text{A} \rightarrow \text{B} \rightarrow \text{C}$. This assumption has to be considered in the context of previous investigations conducted in acetonitrile, in which the irradiation of $[\text{RuT1B0}(\text{NO})](\text{PF}_6)_3$ leads to the complete release of $\text{NO}\cdot$, $[\text{RuT1B0}(\text{MeCN})](\text{PF}_6)_2$ being clearly identified as the final photoproduct (Reaction (1)) [23,24]. Importantly, no additional or intermediate species is observed in acetonitrile, in striking contrast with the present investigation. The search for a metastable transient species in the $\text{NO}\cdot$ release process has become a challenging issue for experimentalists, as theoretical investigations have recently suggested that the overall reaction should necessarily imply a mechanism in two steps. Indeed, theoreticians do not consider the singlet excited state (1A^*) generated after a first photon absorption as a dissociative state [25,26]. Therefore, the need of a second photon absorption would rather lead to an overall mechanism depicted in Scheme 1:



Scheme 1. Mechanism in two steps involved in the $\text{NO}\cdot$ release process.

At first, it seems that the anticipated sideways-bonded isomer in Reaction (2), usually called MS2 in the literature [25,26], could be identified with B (Figure 2), which would imply a complex of formula $[\text{Ru}(\text{MeOphtpy})(\text{bpy})(\eta^2\text{-NO})]^{3+}$, in the present case. Nevertheless, and although few examples of such MS2 states have been reported [27–30], they can hardly be stabilized at room temperature. The details of the analyses undertaken towards the full clarification of the nature and interactions of A, B, C species present in the reaction mixture will be reported as follows: (1) nature of form C; (2) nature of form B, (3) origin of form C, and (4) origin of form B.

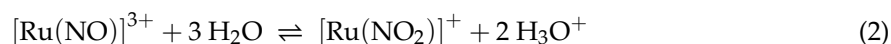
2.1.1. Nature of Form C

The final compound C can be isolated quantitatively after an irradiation of few hours (Figure 2b), and therefore is easily characterized by $^1\text{H-NMR}$ spectroscopy, mass spectrometry, and X-ray diffraction analyses. The crystal structure, described in a following section, reveals that C corresponds to the expected photo-product of formula $[\text{Ru}(\text{MeOphtpy})(\text{bpy})(\text{DMSO}_{(\text{S})})](\text{PF}_6)_2$, in which $\text{DMSO}_{(\text{S})}$ indicates

that a molecule of DMSO is linked to the complex through a Ru-S bond. The NO· release can also be followed by EPR spectroscopy, as it has been already controlled in a previous investigation [23]. To further establish that C arises from the quantitative substitution of NO· by DMSO, the complex $[\text{RuT1B0}(\text{DMSO})_{(\text{S})}]^{2+}$ has been synthesized directly from $[\text{RuT1B0}(\text{Cl})]^+$ (see Experimental Section). It turns out from mass spectrometry and NMR spectroscopy that both chemically and photo-chemically synthesized derivatives are indeed the same species. Infrared spectroscopy provides further evidence for the quantitative replacement of NO· by DMSO in compound C, with the disappearance of the νNO stretching frequency at 1940 cm^{-1} [23,24] and the concomitant appearance of the νSO band at 1101 cm^{-1} .

2.1.2. Nature of Form B

Defining the nature of B is hampered by the fact that it appears difficult to generate this intermediate in sufficient yield and furthermore from the fact that its concentration decreases rapidly in the solution mixture (Figure 2b). To overcome this difficulty, an additional investigation has been conducted on the reference compound $[\text{RuT0B0}(\text{NO})](\text{PF}_6)_3$, the crystal structure of which will be presented in the next section. Contrary to the situation encountered in $[\text{RuT1B0}(\text{NO})](\text{PF}_6)_3$, the photo-generation of C appears more difficult in $[\text{RuT0B0}(\text{NO})](\text{PF}_6)_3$, therefore B can be obtained in high yield (89%) in the reaction mixture, which favors its investigation. Mass spectrometry analyses lead to the conclusion that form B corresponds to $[\text{RuT0B0}(\text{NO}_2)](\text{PF}_6)$, a species which can be generated from A, according to the following acid/base equation:



In order to further characterize B, it is interesting to note that the ^1H -NMR chemical shifts of the bipyridine ligands are only weakly affected by the substituents present on the terpyridine moieties. Therefore, the chemical shifts related to the bipyridine fragments are assumed to be the same in $[\text{RuT0B0}(\text{NO})](\text{PF}_6)_3$ and in $[\text{RuT1B0}(\text{NO})](\text{PF}_6)_3$. The relevant ^1H -NMR chemical shifts are shown in Table 1, where the different X ligands corresponds to those present during the synthetic route towards the $[\text{Ru}(\text{NO})]$ complexes.

Table 1. Chemical shifts of protons in position 6 on the bipyridine ligands, in the case of compounds with unsubstituted ($[\text{RuT0B0}(\text{X})](\text{PF}_6)_3$) and methoxyphenyl-substituted ($[\text{RuT1B0}(\text{X})](\text{PF}_6)_3$) terpyridine.

Ligand X	$[\text{RuT0B0}(\text{X})](\text{PF}_6)_3$	$[\text{RuT1B0}(\text{X})](\text{PF}_6)_3$
Cl^-	10.20 ppm	10.26 ppm
NO_2^- (form B)	9.755 ppm	9.77 ppm ^a
NO (form A)	9.47 ppm	9.50 ppm ^a

^a data from the NMR spectra shown in Figure 2.

The data indicate that the non-isolated form B in $[\text{RuT1B0}(\text{NO})](\text{PF}_6)_3$ (Figure 2), and the related form B in $[\text{RuT0B0}(\text{NO})](\text{PF}_6)_3$ correspond to the same coordination sphere. Therefore B is identified to the ruthenium complex in which NO is switched to NO_2 , in both cases.

Additional support for identifying unambiguously the nature of form B from the available ^1H -NMR data, is provided by a computational investigation. The theoretical characterization of the A, B and C forms was performed by optimizing the geometrical structures of these species for the $[\text{RuT1B0}(\text{NO})]^{3+}$ complex and by computing the ^1H -NMR chemical shifts at the H-6 position. This analysis was also carried out for other intermediate structures and photoproducts potentially produced after photoexcitation. In particular, the $[\text{Ru}(\text{MeOphtpy})(\text{bpy})(\eta^2\text{-NO})]^{3+}$ intermediate (Scheme 1), the $[\text{Ru}(\text{MeOphtpy})(\text{bpy})(\text{ON})]^{3+}$ photoproduct of the linkage N \rightarrow O isomerization of form A and the $[\text{Ru}(\text{MeOphtpy})(\text{bpy})(\text{DMSO}_{(\text{O})})]^{2+}$ species resulting from the linkage S \rightarrow O isomerization of form C [15–19], were all considered. The different structures are reported in Supplementary Materials

along with their respective thermal stabilities. The computed relative $^1\text{H-NMR}$ chemical shifts at the H-6 position of all these species are given in Table 2 with respect to the value of this chemical shift for the initial A form. Experimentally, there is an increase of the chemical shift (deshielding) at the H-6 position on going from A to B by about 0.3 ppm (Figure 2, Table 1). This rules out the $[\text{Ru}(\text{MeOphtpy})(\text{bpy})(\eta^2\text{-NO})]^{3+}$ and $[\text{Ru}(\text{MeOphtpy})(\text{bpy})(\text{ON})]^{3+}$ species for which a shielding is predicted by the computation. Moreover, a further 0.2 ppm deshielding is observed from B to C (Figure 2). This is qualitatively consistent with the variation of the chemical shift from $[\text{RuT0B0}(\text{NO}_2)]^+$ to $[\text{Ru}(\text{MeOphtpy})(\text{bpy})(\text{DMSO}_{(\text{S})})]^{2+}$, in agreement with the experimental characterizations of the B and C forms.

Table 2. Relative chemical shift of protons in position 6 on the bipyridine ligands with respect to the A form of complex $[\text{RuT1B0}(\text{NO})]^{3+}$.

Structures	$\Delta(\delta^{\text{H-6}})$
$[\text{RuT1B0}(\eta^2\text{-NO})]^{3+}$	−0.33 ppm
$[\text{RuT1B0}(\text{ON})]^{3+}$	−0.14 ppm
$[\text{RuT1B0}(\text{NO}_2)]^+$	+0.93 ppm
$[\text{RuT1B0}(\text{DMSO}_{(\text{S})})]^{2+}$	+1.34 ppm
$[\text{RuT1B0}(\text{DMSO}_{(\text{O})})]^{2+}$	+0.74 ppm

In addition, the nature of form B is also confirmed by the analysis of the UV-vis absorption spectra. The experimental spectra were recorded for freshly prepared compounds without irradiation. The spectra are shown in Figure 3 for $[\text{RuT0B0}(\text{NO})]^{3+}$ and $[\text{RuT1B0}(\text{NO})]^{3+}$. From the time evolution of these spectra in the dark, it is clear that these complexes are not thermally stable in DMSO. The presence of two isosbestic points indicates a chemical transformation from A to B without intermediate.

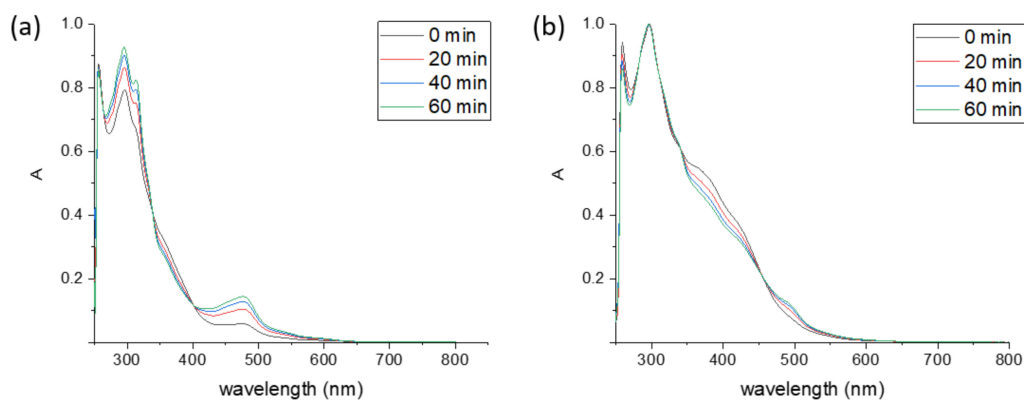


Figure 3. Time-evolution of UV-vis absorption spectra during 1 h without irradiation of (a) $[\text{RuT0B0}(\text{NO})]^{3+}$ and of (b) $[\text{RuT1B0}(\text{NO})]^{3+}$.

To further validate the assignment of B as the $[\text{Ru}(\text{NO}_2)]$ complex, we have computed the UV-vis absorption spectra of $[\text{RuT0B0}(\text{NO})]^{3+}$ and of $[\text{RuT0B0}(\text{NO}_2)]^+$, which appear significantly different according to the experimental data available (Figure 3a). The spectra are shown in Figure 4. The spectrum of $[\text{RuT0B0}(\text{NO})]^{3+}$ is characterized by a weak absorption around $\lambda = 410$ nm and the most intense peak occurs at $\lambda = 290$ nm with a shoulder around 330 nm. Regarding the $[\text{RuT0B0}(\text{NO}_2)]^+$ spectrum, there is also an absorption band in the 440 nm region but it is more intense than that of $[\text{RuT0B0}(\text{NO})]^{3+}$ by a factor ~ 3.5 . The most intense band peaks at $\lambda = 290$ nm as for $[\text{RuT0B0}(\text{NO})]^{3+}$ but it is broader and more intense. Figure 4 also shows some mixed absorption spectra by combining the $[\text{RuT0B0}(\text{NO})]^{3+}$ and $[\text{RuT0B0}(\text{NO}_2)]^+$ spectra. These results are consistent with the time-evolution of the UV-vis absorption spectra shown in Figure 3a, in which a clear absorption increase is observed

for the first and third bands, and a slight decrease of the absorption occurs in the intermediate region, resulting in two isosbestic points.

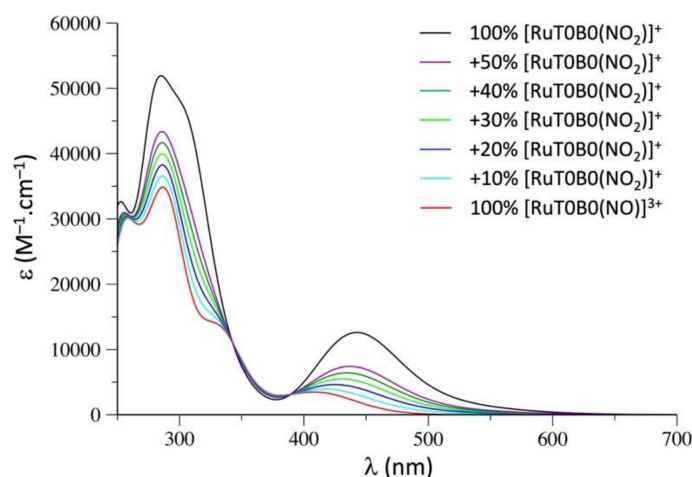


Figure 4. Simulated UV-vis absorption spectra of $[\text{RuT0B0}(\text{NO})]^{3+}$ (red curve) and of $[\text{RuT0B0}(\text{NO}_2)]^+$ (black curve). Mixed spectra adding 10%, 20%, 30%, 40% and 50% of $[\text{RuT0B0}(\text{NO}_2)]^+$ to $[\text{RuT0B0}(\text{NO})]^{3+}$ are shown.

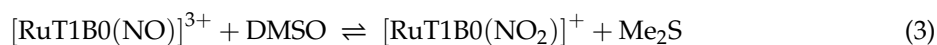
2.1.3. Origin of Form C

A, B, and C being identified precisely, the relevance of the Scheme 1 becomes questionable. In other words, the origin of C, either from A or from B, must be reconsidered. To clarify this issue, a more careful examination of Figure 2a is necessary. If C arises from the hypothetical form B (initial expectation), the kinetics of its formation must reflect the concentration of B, and the slope of [C] drawn against time (T) (Figure 2b) must be equal to 0 when $T = 0$. Additional experiments carried out in the very first few minutes of irradiations (see Supporting Information) reveals that the maximum of the slope is precisely observed at $T = 0$, where the concentration of A is maximum and that of B is equal to 0. Therefore, it becomes clear that C is mainly produced by A instead of B. Nevertheless, and to verify if B takes part in the generation of C, some pure $[\text{RuT1B0}(\text{NO}_2)](\text{PF}_6)$ (form B) was prepared (see Experimental Section). An NMR investigation was carried out in the presence of trimethylamine to avoid the formation of A (back reaction in the acid/base equation 3). After two days of irradiation at $\lambda = 365$ nm, only 10.5% of B was found to be converted to C, however without $\text{NO}\cdot$ generation and without interest for biological purpose. Therefore, although the $B \rightarrow C$ transformation cannot be excluded, one must conclude that C is largely generated by the photoreaction of A.

2.1.4. Origin of Form B

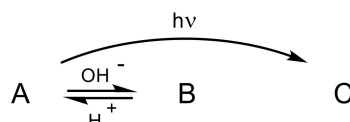
The unexpected production of B from A, observed even in the dark, rises the issue of the mechanism of this reaction. The $[\text{Ru}(\text{NO})] \rightarrow [\text{Ru}(\text{NO}_2)]$ reaction depicted in Equation (3) corresponds to the acid/base equilibrium frequently observed in water medium, but we have never observed it in dry solvents, so far. It suggests either an ultra-fast reactivity with traces of moisture in DMSO, or a chemical reactivity with DMSO. A previous investigation has related the stability of $[\text{Ru}(\text{NO})]$ species in the presence of water to their ν_{NO} IR frequencies [31]. It was predicted that ν_{NO} frequencies above the $1900\text{--}1920$ cm^{-1} range implies high degree of positive charge on the nitrosyl, which becomes very sensitive to nucleophilic attack of the solvent, thus leading to the $\text{NO} \rightarrow \text{NO}_2$ conversion illustrated in Equation (2). We observed here ν_{NO} values of 1940 cm^{-1} and 1945 cm^{-1} for $[\text{RuT0B0}(\text{NO})](\text{PF}_6)_3$ and $[\text{RuT1B0}(\text{NO})](\text{PF}_6)_3$, respectively, which is consistent with some $[\text{Ru}(\text{NO}_2)]$ generation. On the other hand, we have performed our experiments in deuterated DMSO, where the amount of residual water is estimated to be $\leq 0.1\%$. Under such conditions, the $[\text{Ru}(\text{NO})] \rightleftharpoons [\text{Ru}(\text{NO}_2)]$ reaction cannot be strictly avoided, but it is not observed in other deuterated solvents (e.g., acetonitrile) containing the

same amount of residual water, which seems to prove that the nature of the solvent is essential. At this point, it has to be considered that DMSO itself may be an alternative source of oxygen, according to the following equation [32–36]:



However, this possibility which corresponds to a reduction of DMSO is not fully satisfactory in the present case, the $[\text{Ru}(\text{NO})]^{3+} \rightarrow [\text{Ru}(\text{NO}_2)]^+$ reaction being a non-redox process. On the other hand, DMSO is also known as a Lewis bases which, as potential proton trap, could favor the appearance of OH^- and therefore the generation of $[\text{Ru}(\text{NO}_2)]$ species, according to the acid-base Equation (2). To verify this hypothesis, we have observed that, in the reference $[\text{RuT0B0}(\text{NO})]^{3+}$ complex, where forms A and B can be present in DMSO solution with a very small amount of C, the addition of few drops of HPF_6 , leads to the $\text{B} \rightarrow \text{A}$ back conversion. This evolution allows to conclude that the $\text{A} \rightleftharpoons \text{B}$ equilibrium observed in the present species is indeed an acid-base process.

In summary, the various investigations undertaken to rationalize the possible conversions between compounds A, B, and C, suggest that the initial $\text{A} \rightarrow \text{B} \rightarrow \text{C}$ reaction must be replaced by the following Scheme 2:



Scheme 2. Possible interconversion between A, B, and C, under irradiation of A in DMSO.

2.2. Crystal Structures Description

X-ray crystal structures were obtained for $[\text{RuT0B0}(\text{NO})](\text{PF}_6)_3$ (form A) and $[\text{RuT1B0}(\text{DMSO}_{(s)})](\text{PF}_6)_2$ (form C). The main crystal data are gathered in Table 3 for both compounds.

Table 3. Crystal data for $[\text{RuT0B0}(\text{NO})](\text{PF}_6)_3$, and $[\text{RuT1B0}(\text{DMSO}_{(s)})](\text{PF}_6)_2$.

	$[\text{RuT0B0}(\text{NO})](\text{PF}_6)_3$ $\frac{1}{2} \text{CH}_2\text{Cl}_2\text{-H}_2\text{O}$	$[\text{RuT1B0}(\text{DMSO}_{(s)})](\text{PF}_6)_2$ CH_3CN
Chemical formula	$\text{C}_{25.5}\text{H}_{22}\text{ClF}_{18}\text{N}_6\text{O}_2\text{P}_3\text{Ru}$	$\text{C}_{36}\text{H}_{34}\text{F}_{12}\text{N}_6\text{O}_2\text{P}_2\text{RuS}_1$
Molecular weight (g/mol)	1015.90	1005.76
Crystal system	monoclinic	triclinic
Space group	$\text{P}2_1/\text{n}$	P-1
a (Å)	19.2309(9)	12.6477(6)
b (Å)	19.2739(10)	13.2076(5)
c (Å)	19.7628(10)	13.2282(7)
a (deg)	90	97.4744(14)
b (deg)	106.5407(17)	109.0108(14)
g (deg)	90	106.0250(14)
V (Å ³)	7022.0(6)	1948.27(16)
Z	8	2
T (K)	110	113
μ (MoK α)	0.793	0.639
D_{calc} (g/cm ³)	1.92	1.71
T (K)	110	113
Reflect. measured	173754	99152
2 θ range	$1.30^\circ \leq 2\theta \leq 28.34^\circ$	$1.65^\circ \leq 2\theta \leq 30.61^\circ$
Reflect. unique	17439	11796
Rint	0.0777	0.0432
Refinement on	F	F
Nb Parameters	1048	541
R1 (I > n σ (I))	0.0767, n = 2.5	0.0294, n = 3
wR2 (I > n σ (I))	0.0964, n = 2.5	0.0305, n = 3
Residual electron density ($\bar{e}\cdot\text{Å}^{-3}$)	4.41/−1.77	1.02/−0.91

[RuT0B0(NO)](PF₆)₃ crystallizes in the P2₁/n monoclinic space group. The asymmetric unit cell, shown in Figure 5, is built up from two ruthenium centers, six PF₆[−] counter ions, one molecule of dichloromethane and two molecules of water, the presence of which can be explained by the fact that the solvent used for the diffusion experiment was standard acetonitrile in which some amount of water is always present. The presence of three PF₆[−] per ruthenium confirms the 3+ charge of the complex, which corresponds to {Ru-NO}⁶ in the Enemark notation, where 6 is the sum of the electrons present in the *d* orbitals of Ru and those in the π* orbitals of NO [37]. The torsion angle between the mean plane of terpyridine ligand (15 C + 3 N atoms) and that of the bipyridine (10 C + 2 N atoms) is equal to 87.97 deg. and 87.07 deg., for complexes 1 (Ru1) and 2 (Ru2), respectively (Figure 4). The four terpyridine and bipyridine ligands are roughly planar with largest distance to mean plane observed at 0.190 Å, for the C2 atom of the bipyridine of complex 1 (Ru1). Selected bonds and angles for the first coordination sphere of the ruthenium complexes are gathered in Table 4. Although chemically different, the two ruthenium complexes exhibit similar coordination spheres, the shortest Ru-pyridine distance being observed at the central pyridine of the terpyridine ligands. The Ru-N-O angles are close to 180° in both complexes, which indicates for {Ru-NO}⁶ an electronic structure which corresponds to Ru^{II}-(NO)⁺ [38].

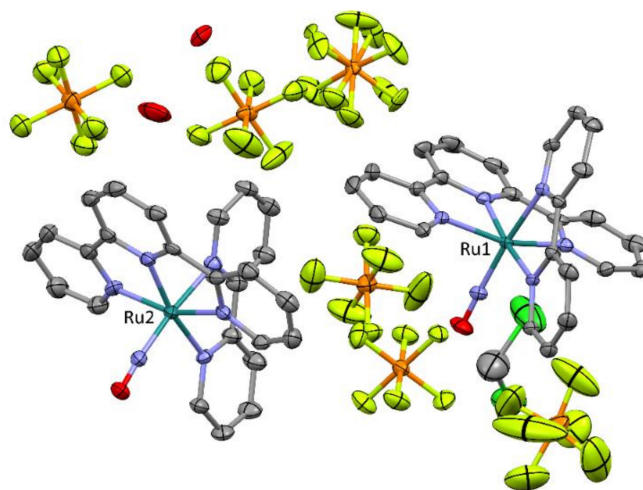


Figure 5. Asymmetric unit for [RuT0B0(NO)](PF₆)₃ · $\frac{1}{2}$ CH₂Cl₂–H₂O. Displacement ellipsoids are drawn at the 50% probability level. Hydrogen atoms are omitted for clarity.

Table 4. Selected bond lengths (in Å) and angles (in deg.) in [RuT0B0(NO)]³⁺, and [RuT1B0(DMSO_(S))]²⁺.

	[RuT0B0(NO)] ³⁺		[RuT1B0(DMSO _(S))] ²⁺
	Complex 1 (Ru1)	Complex 2 (Ru2)	
<i>Ru-NO</i>			
Ru-N	1.766(6)	1.770(7)	
N-O	1.119(8)	1.135(9)	
Ru-N-O	177.7(6)	175.3(6)	
<i>Ru-DMSO</i>			
Ru-S			2.2666(4)
S-O			1.4826(12)
<i>Ru-tpy</i>			
Ru-N _{central}	1.998(6)	1.996(6)	1.9735(12)
Ru-N _{lateral}	2.093(6)	2.064(7)	2.0738(12)
	2.101(6)	2.084(7)	2.0842(12)
<i>Ru-bpy</i>			
Ru-N _{transNO}	2.082(6)	2.092(7)	
Ru-N _{transDMSO}			2.0912(12)
Ru-N	2.089(6)	2.077(6)	2.1037(12)

[RuT1B0(DMSO_(S))](PF₆)₂ (form C) crystallizes in the P-1 triclinic space group. The asymmetric unit cell (Figure 6) is built up from one ruthenium complex, two PF₆[−], and one molecule of acetonitrile. The presence of two PF₆[−] indicate that the oxidation of the metal center corresponds to Ru^{II}. The torsion angle between the mean plane of terpyridine ligand and that of the bipyridine is equal to 89.07 deg. As observed in [RuT0B0(NO)]³⁺, the terpyridine and the bipyridine ligands are roughly planar with largest distance to mean plan observed at 0.122 Å, for the C24 atom of the bipyridine. The coordination sphere of [RuT1B0(DMSO_(S))]²⁺ is described in Table 4. The S-O bond length of the DMSO ligand is equal to 1.4826(12) Å which is longer than that of 1.46(3) Å observed in the previously reported structure of [RuT0B0(DMSO_(S))](SO₃CF₃)₂ [39]. The torsion angle between the methoxyphenyl substituent and the terpyridine is equal to 20.95°, which allows a significant π overlap between the rings.

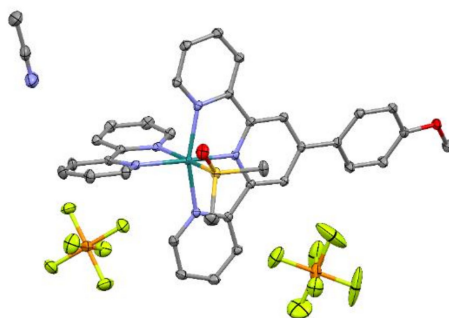


Figure 6. Asymmetric unit for [RuT1B0(DMSO_(S))](PF₆)₂ · CH₃CN. Displacement ellipsoids are drawn at the 50% probability level. Hydrogen atoms are omitted for clarity.

At first, the presence of a Ru^{II} metal center in the photoproduct is surprising, based on Equation (1), which, in the present case, should be written as follows:



An alternative would be to consider the following undesirable equation:



Nevertheless, the observation of NO⁺ release from [Ru(R-tpy)(bpy)(NO)]³⁺ complexes was never observed [23,24,40,41], leading to the conclusion that a fast Ru^{III} → Ru^{II} reduction occurs in the [Ru^{III}(solvent)]³⁺ species when five pyridines (tpy + bpy) are present in the coordination sphere, a possibility which has been discussed elsewhere [23].

2.3. Photochemical Behavior of [Ru(R-tpy)(bpy)(NO)]³⁺ in DMSO: the Second Step

While the A to C transformation is completed within a couple of hours (Figure 2), it is interesting to observe that an additional but very slow phenomenon takes place under continuous irradiation of the reaction mixture. This general evolution is exemplified in Figure 7, where the ¹H-NMR signal of atom H-6 of the bipyridine ligand, is presented at various times during an irradiation of a sample of [RuT0B0(NO)](PF₆)₃. As the starting [RuT0B0(NO)](PF₆)₃ exhibits a single doublet at δ = 9.47 ppm (Figure 7a), 1.5 h of irradiation leads to its almost complete conversion to B and C (Figure 7b), an evaluation fully consistent with the experiment described in Figure 2 for [RuT1B0(NO)](PF₆)₃. Interestingly, a new doublet identified as form D in this figure appears at 9.49 ppm. However, its concentration remains very low (4%). After 5 h of irradiation (Figure 7c), most of the conversion of A to C is achieved, the B → C reaction being very slow. Nevertheless, the concentration of the new form D rises to 14.9%. At this point, when the reaction mixture is kept in the dark for 3 h (Figure 7d), the new form D completely disappears, which indicate a D → C transformation in the dark. Interestingly, an additional irradiation of 13 h leads to the restoration of the situation observed in

Figure 7c. Altogether, these experiments indicate that D is formed by irradiation of C, the process being slow and completely reversible in the dark. The overall photoreaction process is summarized in Scheme 3.

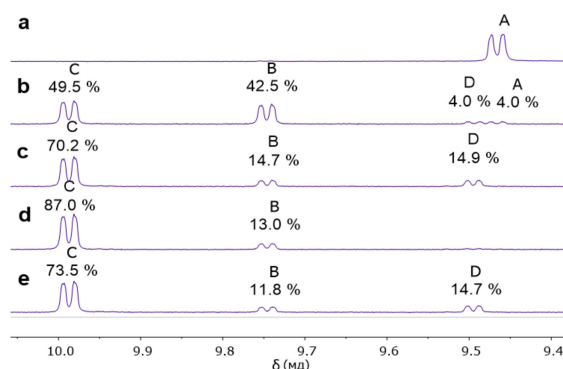
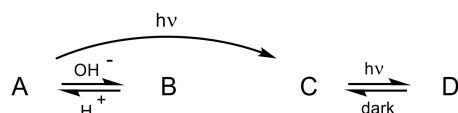


Figure 7. $^1\text{H-NMR}$ spectra in DMSO for $[\text{RuT0B0}(\text{NO})](\text{PF}_6)_3$ with relative intensities: (a) starting compound (form A); (b) after 1.5 h of irradiation; (c) after 5 h of irradiation; (d) after keeping the resulting sample 3 h in the dark; (e) after an additional 13 h of irradiation. H-6 is selected as being the most sensitive to the nature of the X ligand present in $[\text{Ru}(\text{tpy})(\text{bpy})(\text{X})]^{n+}$ entities.



Scheme 3. Complete interconversion between forms A, B, C, and D in DMSO.

It can be inferred from the above experiment that D is a photo-isomerized form of $[\text{RuT0B0}(\text{DMSO}_{(\text{S})})]^{2+}$, which can be identified as $[\text{RuT0B0}(\text{DMSO}_{(\text{O})})]^{2+}$. Indeed, the Ru-S to Ru-O linkage isomerization of ruthenium-polypyridine sulfoxide complexes has previously been reported, and thoroughly reviewed [20,42,43]. The assignment of the D form is here supported by our theoretical calculations of the $^1\text{H-NMR}$ chemical shifts. The decrease of the chemical shift (shielding) for H-6 on going from C to D is computed to be 0.6 ppm for the T1B0 complex (Table 2), which is in good agreement with the shielding of ca. 0.5 ppm observed experimentally in the T0B0 complex (Figure 7).

A literature survey reveals that the S \rightarrow O linkage isomerization of Ru-DMSO species was first triggered electrochemically [44,45]. The observed tendency is that polarizable Ru^{II} metal centers exhibit a preference for the π -acceptor S-bonded DMSO, while O-bonded forms are stabilized by Ru^{III} species. In the case of the present investigation and as the metal centers are in oxidation state II, the possibility for linkage isomerization to the metastable Ru-DMSO_(O) isomers is naturally addressed. In the case of $[\text{RuT0B0}(\text{DMSO}_{(\text{S})})]^{2+}$, the complete characterization of D is not possible because this species appears rather unstable and is always present as a small amount in the reaction mixture.

In an attempt to try to find a correlation between the rate of Ru-DMSO_(S) \rightarrow Ru-DMSO_(O) photo-isomerization and the electronic structures of the complexes, $[\text{RuT0B0}(\text{DMSO}_{(\text{S})})]^{2+}$ and $[\text{RuT1B0}(\text{DMSO}_{(\text{S})})]^{2+}$ were investigated together with additional ruthenium complexes. In these new species, so called $[\text{RuT2B0}(\text{DMSO}_{(\text{S})})]^{2+}$ and $[\text{RuT3B0}(\text{DMSO}_{(\text{S})})]^{2+}$ (Figure 1), Br and NO₂ substituents are present, respectively, to modulate the intramolecular charge transfer capabilities. These investigations were carried out on pure complexes in the C form (Ru-DMSO_(S)), obtained by direct chemical synthesis (see Materials and Methods). The irradiations were performed for several hours, in order to reach the Ru-DMSO_(S) \rightleftharpoons Ru-DMSO_(O) equilibrium, which was observed to be achieved within one hour for the four complexes under investigation. The Ru-DMSO_(O)/Ru-DMSO_(S) ratios are presented in Table 5. It appears from these experiments that the more donating substituent (MeO in $[\text{RuT1B0}(\text{DMSO}_{(\text{S})})]^{2+}$) leads to the lowest ratio of isomerization (25%), while the more withdrawing substituent (NO₂ in $[\text{RuT3B0}(\text{DMSO}_{(\text{S})})]^{2+}$) leads to the highest ratio (46%). This result is counterintuitive with respect to the natural assumption that stronger charge transfers toward the

Ru-DMSO fragment should encourage more efficient linkage isomerizations in these species. However, it is known that triplet metal centered d-d states play a crucial role in the photo-isomerization mechanism of ruthenium sulfoxide complexes [15,18,46]. In addition, the respective absorption properties of the Ru-DMSO_(O) and Ru-DMSO_(S) will play a role in the photoconversion yield. Thus, this simple reasoning cannot be used.

In an alternative approach the DMSO_(O)/DMSO_(S) ratio can be tentatively related to the absorbance of both species at the wavelength of irradiation ($\lambda = 365$ nm). Along this line, and assuming that the quantum yield of photo-isomerization is similar for DMSO_(S) $\xrightarrow{h\nu}$ DMSO_(O) and for DMSO_(O) $\xrightarrow{h\nu}$ DMSO_(S) photoreactions, the equilibrium is expected when the absorbance (extinction coefficient (ϵ) \times concentration) is the same for both DMSO_(O) and DMSO_(S) species, leading to the following equation:

$$\epsilon(\text{Ru-DMSO}_{(S)}) \times [\text{Ru-DMSO}_{(S)}] \approx \epsilon(\text{Ru-DMSO}_{(O)}) \times [\text{Ru-DMSO}_{(O)}] \quad (6)$$

Table 5. Comparison of the Ru-DMSO_(O)/Ru-DMSO_(S) ratios determined by ¹H-NMR spectroscopy after one hour of irradiation of ruthenium complexes with various substituted terpyridine ligands at $\lambda = 365$ nm.

Complex	Substituent on Terpyridine	Ru-DMSO _(O) /Ru-DMSO _(S)		Computed ϵ_{365} (L mol ⁻¹ cm ⁻¹)
		Experimental ¹	Computed ²	
[RuT0B0(DMSO(S))] ²⁺	H	42%	53%	6021
[RuT0B0(DMSO(O))] ²⁺	H			5317
[RuT1B0(DMSO(S))] ²⁺	MeO-phenyl	25%	32%	9806
[RuT1B0(DMSO(O))] ²⁺	MeO-phenyl			21,112
[RuT2B0(DMSO(S))] ²⁺	Br-phenyl	31%	47%	12,365
[RuT2B0(DMSO(S))] ²⁺	Br-phenyl			14,186
[RuT3B0(DMSO(S))] ²⁺	NO ₂ -phenyl	46%	64%	14,034
[RuT3B0(DMSO(S))] ²⁺	NO ₂ -phenyl			7794

¹ determined by ¹H-NMR spectroscopy under irradiation. ² determined by the ratio of the extinction coefficient computed at $\lambda = 365$ nm.

To verify this hypothesis, the UV-visible spectra of Ru-DMSO_(S), and Ru-DMSO_(O) complexes have to be examined. No UV-visible data being available for the Ru-DMSO_(O) isomers, which cannot be isolated, the comparison had to be carried out on computed spectra. Nevertheless, the accuracy of the computation can be tested with the experimental spectra available for the Ru-DMSO_(S) forms, gathered in Figure 8.

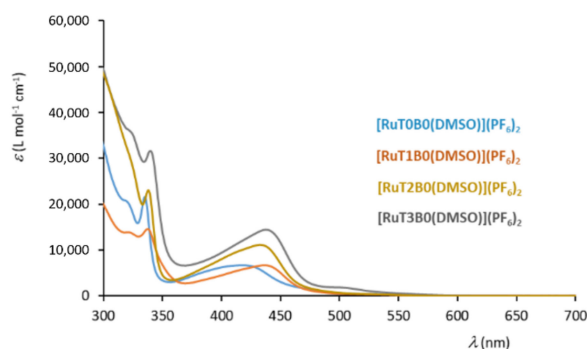


Figure 8. UV-visible spectra in acetonitrile for the four Ru-DMSO_(S) complexes.

Experimentally, the four Ru-DMSO_(S) compounds exhibit a low energy transition with absorption maxima in the $\lambda = 415$ – 440 nm range, more intense transitions being present at higher energy. This general feature is confirmed by the simulated spectra (Supplementary Materials), for which a slight blue shift not exceeding 1500 cm⁻¹ (<0.2 eV) is obtained for the low-lying transitions compared

to the experimental spectra. Therefore, the agreement between computations and experiments appears satisfactory, which supports the reliability of the computational approach. The main features of the computed spectra are shown in Table 6.

Table 6. Computed absorption maxima (λ_{\max} in nm), oscillator strength (f), composition and main character of the low-energy transition of the Ru-DMSO_(S) and Ru-DMSO_(O) complexes, compared with the experimental data available.

Compound	UV-vis		DFT Computed Data					
	λ_{\max}	ϵ	Transition ^a	λ	f	λ_{\max} ^b	Composition ^c	Character ^d
[RuT0B0(DMSO _(S))] ²⁺	419	6680	S ₀ → S ₆	395	0.104	395	0.53 $\chi_{129} \rightarrow 132$ + 0.41 $\chi_{129} \rightarrow 133$	Ru(d) → π (bpy/tpy)
[RuT0B0(DMSO _(O))] ²⁺			S ₀ → S ₆	462	0.103	456	0.38 $\chi_{128} \rightarrow 133$ - 0.32 $\chi_{129} \rightarrow 1313$	Ru(d) → π (tpy)
[RuT1B0(DMSO _(S))] ²⁺	436	6680	S ₀ → S ₃	440	0.311	430	0.61 $\chi_{158} \rightarrow 159$	π (PhOMe)Ru(d) → π (tpy)
[RuT1B0(DMSO _(O))] ²⁺			S ₀ → S ₆	474	0.134	472	0.40 $\chi_{158} \rightarrow 161$ + 0.35 $\chi_{158} \rightarrow 160$	π (PhOMe)Ru(d) → π (tpy)
[RuT2B0(DMSO _(S))] ²⁺	433	11150	S ₀ → S ₄	427	0.159	409	0.53 $\chi_{167} \rightarrow 170$ - 0.42 $\chi_{165} \rightarrow 168$	Ru(d) → π (bpy)
[RuT2B0(DMSO _(O))] ²⁺			S ₀ → S ₆	470	0.154	466	0.35 $\chi_{167} \rightarrow 169$ - 0.34 $\chi_{166} \rightarrow 168$	Ru(d) → π (tpy)
[RuT3B0(DMSO _(S))] ²⁺	438	14500	S ₀ → S ₄	432	0.210	412	0.56 $\chi_{159} \rightarrow 162$	Ru(d) → π (tpyPhNO ₂)
[RuT3B0(DMSO _(O))] ²⁺			S ₀ → S ₅	477	0.181	478	0.34 $\chi_{161} \rightarrow 164$ + 0.32 $\chi_{161} \rightarrow 163$	Ru(d) → π (tpyPhNO ₂)

^a Main transition bearing the first absorption band. ^b Computed absorption maximum of the first absorption band of the simulated spectra (see Supplementary Information). ^c Main excitations involved in the electronic transition.

^d Main character deduced from the natural transition orbitals (shown in Supplementary Information).

The computed extinction coefficients at 365 nm lead to the Ru-DMSO_(O)/Ru-DMSO_(S) ratio gathered in Table 5. The values substantially agree with the experiment and confirm that the most electron withdrawing substituent (NO₂-phenyl) leads to the more efficient Ru-DMSO_(S) → Ru-DMSO_(O) isomerization process. With this respect, the difference in absorption occurring during the linkage isomerization appears to be a key parameter to explain the concentration of Ru-DMSO_(O) at the equilibrium.

3. Materials and Methods

3.1. Starting Materials and Equipment

The starting chemicals 2-acetylpyridine, NH₄PF₆ and 2,2':6',2''-terpyridine were purchased from Alfa-Aesar (Haverhill, MA, USA). Hexafluorophosphoric acid (~65% in H₂O) was from Sigma-Aldrich (Tharabie, France), 2,2'-bipyridine from TCI (TCI Europe N.V., Zwijndrecht, Belgium), RuCl₃·xH₂O from Strem Chemicals (Bischheim, France), 4-methoxybenzaldehyde, triethylamine and trimethylamine from Acros Organics (Fisher Scientific, Geel, Belgium), and NaNO₂ from Fluka (Saint-Quentin-Fallavier, France). Chemicals and solvents were analytical grade and used without further purification. [RuT0B0(NO)](PF₆)₃, and [RuT1B0(NO)](PF₆)₃ (forms A) were prepared following the procedure previously reported by Meyer [47,48], and by our group [23], respectively. [RuT1B0(NO₂)](PF₆)₃ (form B) was prepared chemically as an intermediate towards the synthesis of [RuT1B0(NO)](PF₆)₃ [23]. Bromophenylterpyridine [49] and nitrophenylterpyridine [50] were prepared as previously described.

Elemental analyses were performed at LCC with a 2400 series II Instrument (Perkin-Elmer, Waltham, MA, USA). UV-Vis spectra were obtained on a Perkin Elmer Lambda 35 UV-Vis spectrometer (Perkin-Elmer, Waltham, MA, USA). Irradiation experiments were achieved on 8–9 milligrams on ruthenium complexes dissolved in 0.6 mL of DMSO-*d*₆ in a NMR tube with a LED-lamp operating at $\lambda = 365$ nm or 395 nm, under constant fanning. The experiments were carried out in the NMR room, and the composition of the reaction mixtures were recorded periodically by ¹H-NMR spectroscopy. The time required for transferring the samples to the spectrometer were restricted to few seconds. The ¹H-NMR spectra were recorded in DMSO-*d*₆, on an Avance 400 Bruker spectrometer (Bruker-France, Wissembourg 67160). The complete assignment for the ruthenium complexes are provided in

Supplementary Materials (Figures S1,S2). In the case of $[\text{RuT1B0}(\text{NO})](\text{PF}_6)_3$, the completeness of the $\text{A} \rightarrow \text{C}$ transformation (95%) was achieved after a time of irradiation of about 7 h. The solution was then transferred into a round-bottomed flask, and evaporated to dryness under vacuum at the Schlenk line, with moderate heating (40–50 °C). The resulting solid was dissolved in 2 mL of acetonitrile, filtered, transferred into a vial and placed in a large beaker in the presence of a flask, filled with a large amount of diethyl ether. Single crystals suitable for X-ray analyses appear within a few days after slow diffusion of diethyl ether into the concentrated solution of C. For the investigation of the direct $\text{C} \rightarrow \text{D}$ transformations (Table 5), the pure ruthenium-DMSO_(S) complexes (form C) were diluted to $3 \times 10^{-3} \text{ mol}\cdot\text{L}^{-1}$ and fully irradiated for several hours in a vial under stirring, and checked regularly by $^1\text{H-NMR}$. The C/D equilibrium was reached within one hour of irradiation, in any cases.

3.2. Synthesis of Ru-DMSO Complexes (Form C)

The four compounds were synthesized from the $[\text{Ru}(\text{R-tpy})\text{bpyCl}](\text{Cl})$ precursors: $[\text{RuT0B0}(\text{Cl})](\text{Cl})$ [51] and $[\text{RuT1B0}(\text{Cl})](\text{Cl})$ [2] were previously reported in the literature. $[\text{RuT2B0}(\text{Cl})](\text{Cl})$ and $[\text{RuT3B0}(\text{Cl})](\text{Cl})$ were synthesized according to the methodology previously reported for $[\text{RuT1B0}(\text{Cl})](\text{Cl})$ [23].

$[\text{RuT2B0Cl}](\text{Cl})$. Starting materials: $[\text{RuT2Cl}_3]$ (425 mg, 0.69 mmol), 2,2'-bipyridine (108 mg, 0.69 mmol), LiCl (165 mg, 3.9 mmol), trimethylamine (0.82 mL, 5.9 mmol), EtOH (48 mL), H₂O (16 mL). Yield: 390 mg, 68%. $^1\text{H-NMR}$ (400 MHz, DMSO-*d*₆) δ 10.11 (dd, $J = 5.7, 1.5 \text{ Hz}$, 1H), 9.22 (s, 2H), 8.95 (dd, $J = 8.3, 5.0 \text{ Hz}$, 3H), 8.66 (d, $J = 8.1 \text{ Hz}$, 1H), 8.41–8.28 (m, 3H), 8.14–7.97 (m, 5H), 7.79 (td, $J = 7.8, 1.4 \text{ Hz}$, 1H), 7.64 (dd, $J = 5.6, 1.5 \text{ Hz}$, 2H), 7.41 (ddd, $J = 7.4, 5.6, 1.3 \text{ Hz}$, 3H), 7.08 (ddd, $J = 7.3, 5.7, 1.3 \text{ Hz}$, 1H).

$[\text{RuT3B0Cl}](\text{Cl})$. Starting materials: $[\text{RuT3Cl}_3]$ (626 mg, 1.1 mmol), 2,2'-bipyridine (174 mg, 1.1 mmol), LiCl (351 mg, 8.4 mmol), trimethylamine (1.31 mL, 9.4 mmol), EtOH (90 mL), H₂O (30 mL). Yield: 578 mg, 66%. $^1\text{H-NMR}$ (400 MHz, methanol-*d*₄) δ 10.26 (ddd, $J = 5.6, 1.6, 0.8 \text{ Hz}$, 1H), 9.04 (s, 2H), 8.84–8.78 (m, 1H), 8.75–8.70 (m, 2H), 8.54–8.49 (m, 3H), 8.45–8.39 (m, 2H), 8.39–8.32 (m, 1H), 8.06 (ddd, $J = 7.6, 5.6, 1.3 \text{ Hz}$, 1H), 8.00–7.93 (m, 2H), 7.80–7.72 (m, 3H), 7.47–7.42 (m, 1H), 7.38 (ddd, $J = 7.6, 5.5, 1.3 \text{ Hz}$, 2H), 7.06 (ddd, $J = 7.3, 5.8, 1.4 \text{ Hz}$, 1H).

3.2.1. $[\text{RuT0B0}(\text{DMSO})_{(S)}](\text{PF}_6)_2$

$[\text{RuT0B0}(\text{Cl})](\text{Cl})$ was first transformed to $[\text{RuT0B0}(\text{Cl})](\text{PF}_6)$ by metathesis, using a 20-fold excess of NH_4PF_6 in water. Then, and following the methodology described by Root and Deutsch [45], $[\text{RuT0B0}(\text{Cl})](\text{PF}_6)$ (83 mg, 0.12 mmol) and AgPF_6 (62 mg, 0.24 mmol), were added to a two-necked flask and connected to a Schlenk line. The flask was filled with argon and deaerated DMSO (8 mL) was added. The resulting solution was stirred for 45 h at 80 °C, then cooled down to room temperature. The AgCl precipitate formed during the reaction was filtered off. Finally, DMSO was evaporated under vacuum resulting of a light-orange powder, which was thoroughly rinsed by toluene, to remove the unreacted AgPF_6 . Yield: 77 mg (0.09 mmol); $\varphi = 75\%$. $^1\text{H-NMR}$ (400 MHz, DMSO-*d*₆) δ 10.03–9.96 (m, 1H), 8.95 (dd, $J = 8.3, 5.1 \text{ Hz}$, 3H), 8.81–8.74 (m, 3H), 8.59 (t, $J = 8.1 \text{ Hz}$, 1H), 8.46 (td, $J = 7.7, 1.3 \text{ Hz}$, 1H), 8.20 (td, $J = 7.9, 1.5 \text{ Hz}$, 2H), 8.15–8.02 (m, 2H), 7.85–7.78 (m, 2H), 7.53 (ddd, $J = 7.0, 5.6, 1.3 \text{ Hz}$, 2H), 7.39–7.30 (m, 1H), 7.16–7.09 (m, 1H). IR: $\nu(\text{S=O}) = 1103 \text{ cm}^{-1}$.

3.2.2. $[\text{RuT1B0}(\text{DMSO})_{(S)}](\text{PF}_6)_2$

The synthesis was achieved following the procedure described above for $[\text{RuT0B0}(\text{DMSO})_{(S)}](\text{PF}_6)_2$. Starting materials: $[\text{RuT1B0}(\text{Cl})](\text{PF}_6)$ (200 mg 0.25 mmol), AgPF_6 (126 mg, 0.5 mmol), DMSO (8 mL). Yield: 204 mg; 85%. $^1\text{H-NMR}$ (400 MHz, DMSO-*d*₆) δ 10.06–9.99 (m, 1H), 9.28 (s, 2H), 9.04 (dd, $J = 8.1, 1.2 \text{ Hz}$, 2H), 8.94 (d, $J = 8.1 \text{ Hz}$, 1H), 8.77 (d, $J = 8.2 \text{ Hz}$, 1H), 8.45 (td, $J = 7.9, 1.5 \text{ Hz}$, 1H), 8.41–8.35 (m, 2H), 8.22 (td, $J = 7.9, 1.5 \text{ Hz}$, 2H), 8.14–8.02 (m, 2H), 7.86–7.78 (m, 2H), 7.53 (ddd, $J = 7.1, 5.6, 1.3 \text{ Hz}$, 2H), 7.35 (ddd, $J = 7.3, 5.7, 1.2 \text{ Hz}$, 1H), 7.32–7.23 (m, 3H). IR: $\nu(\text{S=O}) = 1101 \text{ cm}^{-1}$. MS: $m/z = 337.33$ ($m/z_{\text{theor}}([\text{Ru}(\text{MeOPhtpy})\text{bpyDMSO}]^{2+}) = 337.56$); 819.42 ($m/z_{\text{theor}}([\text{Ru}(\text{MeOPhtpy})\text{bpyDMSO}](\text{PF}_6)^+)$

= 820.08). Anal. Calcd. for $C_{34}H_{31}F_{12}N_5O_2P_2RuS$: C, 42.33; H, 3.24; N, 7.26. Found: C, 42.63; H, 3.33; N, 6.91.

3.2.3. $[RuT2B0(DMSO)_{(S)}](PF_6)_2$

The synthesis was achieved following the procedure described above for $[RuT1B0(DMSO)_{(S)}](PF_6)_2$. Starting materials: $[Ru(BrPhtpy)bpyCl]PF_6$ (283 mg, 0.34 mmol), $AgPF_6$ (174 mg, 0.68 mmol), DMSO (30 mL). Yield: 311 mg (0.31 mmol) 92%. 1H -NMR (400 MHz, $DMSO-d_6$) δ 10.08–10.00 (m, 1H), 9.35 (s, 2H), 9.05 (d, $J = 8.1$ Hz, 2H), 8.95 (d, $J = 8.1$ Hz, 1H), 8.78 (d, $J = 8.4$ Hz, 1H), 8.52–8.42 (m, 1H), 8.40–8.32 (m, 2H), 8.25 (td, $J = 7.9, 1.5$ Hz, 2H), 8.16–8.03 (m, 2H), 8.03–7.95 (m, 2H), 7.84 (dt, $J = 5.5, 1.3$ Hz, 2H), 7.56 (ddd, $J = 7.0, 5.6, 1.3$ Hz, 2H), 7.35 (ddd, $J = 7.3, 5.7, 1.3$ Hz, 1H), 7.31–7.24 (m, 1H). IR: ν (S=O) = 1092 cm^{-1} . MS: $m/z = 362.25$ ($m/z_{theor}([Ru(BrPhtpy)bpyDMSO]^{2+}) = 361.51$); 869.33 ($m/z_{theor}([Ru(BrPhtpy)bpyDMSO](PF_6)^+) = 868.98$). Anal. Calcd. for $C_{33}H_{28}BrF_{12}N_5O_2P_2RuS$: C, 39.10; H, 2.78; N, 6.91. Found: C, 39.13; H, 3.12; N, 6.53.

3.2.4. $[RuT3B0(DMSO)_{(S)}](PF_6)_2$

The synthesis was achieved following the procedure described above for $[RuT0B0(DMSO)_{(S)}](PF_6)_2$. Starting materials: $[Ru(NO_2Phtpy)bpyCl]PF_6$ (101 mg, 0.13 mmol), $AgPF_6$ (66 mg, 0.26 mmol), DMSO (10 mL). Yield: 109 mg (0.11 mmol) 87%. 1H -NMR (400 MHz, $DMSO-d_6$) δ 10.04 (dd, $J = 5.5, 1.3$ Hz, 1H), 9.42 (s, 2H), 9.09–9.03 (m, 2H), 8.95 (d, $J = 8.0$ Hz, 1H), 8.77 (d, $J = 8.2$ Hz, 1H), 8.61 (d, $J = 0.7$ Hz, 4H), 8.46 (td, $J = 7.9, 1.5$ Hz, 1H), 8.26 (td, $J = 7.9, 1.5$ Hz, 2H), 8.16–8.10 (m, 1H), 8.09–8.03 (m, 1H), 7.87–7.81 (m, 2H), 7.57 (ddd, $J = 7.7, 5.5, 1.3$ Hz, 2H), 7.36–7.30 (m, 1H), 7.30–7.25 (m, 1H). IR: ν (S=O) = 1091 cm^{-1} . MS: $m/z = 344.83$ ($m/z_{theor}([Ru(NO_2Phtpy)bpyDMSO]^{2+}) = 345.05$). Anal. Calcd. for $C_{33}H_{28}F_{12}N_6O_3P_2RuS$: C, 40.46; H, 2.88; N, 8.58. Found: C, 40.62; H, 2.68; N, 8.30.

3.3. Synthesis of Form D, by Photo-Isomerization of Form C

Although the photo-generated $Ru-DMSO_{(O)}$ complexes were not isolated, their 1H -NMR spectra (400 MHz, $DMSO-d_6$) are accessible from the C/D mixture (see Supplementary Materials). For $[RuT0B0(DMSO)_{(S)}](PF_6)_2$: δ 9.49 (d, $J = 5.5$ Hz, 1H), 8.98–8.89 (m, 3H), 8.80 (d, $J = 8.2$ Hz, 3H), 8.63 (d, $J = 8.1$ Hz, 1H), 8.39 (d, $J = 8.0$ Hz, 2H), 8.11 (m, 2H), 7.76 (m, 1H), 7.72 (dd, $J = 5.2, 1.4$ Hz, 2H), 7.48 (ddd, $J = 7.4, 5.6, 1.3$ Hz, 2H), 7.28 (d, 1H), 7.07 (t, 1H).

For $[RuT1B0(DMSO)_{(S)}](PF_6)_2$: δ 9.52 (d, $J = 5.5$ Hz, 1H), 9.29 (s, 2H), 9.06 (d, 2H), 8.95 (m, 1H), 8.63 (d, $J = 8.2$ Hz, 1H), 8.14–8.04 (m, 5H), 7.78 (t, 1H), 7.72 (d, $J = 5.4$ Hz, 2H), 7.50–7.45 (t, 2H), 7.38 (d, 1H), 7.27 (m, 3H), 7.07 (t, 1H).

For $[RuT2B0(DMSO)_{(S)}](PF_6)_2$: δ 9.52 (d, $J = 5.5$ Hz, 1H), 9.36 (s, 2H), 9.06 (d, $J = 7.8$ Hz, 2H), 8.97 (d, $J = 9.5$ Hz, 1H), 8.64 (d, $J = 8.1$ Hz, 1H), 8.39 (d, 2H), 8.19–8.14 (m, 3H), 7.96 (d, 2H), 7.79 (t, $J = 7.8$ Hz, 1H), 7.76–7.71 (m, 2H), 7.52–7.47 (m, 2H), 7.37 (m, 2H), 7.10–7.03 (t, 1H).

For $[RuT3B0(DMSO)_{(S)}](PF_6)_2$: δ 9.52 (d, $J = 5.5$ Hz, 1H), 9.44 (s, 2H), 9.08 (d, $J = 9.2$ Hz, 2H), 8.98 (d, 1H), 8.69–8.54 (m, 5H), 8.46 (t, $J = 7.6$ Hz, 1H), 8.21–8.10 (m, 3H), 7.82–7.77 (t, 1H), 7.76–7.73 (d, 2H), 7.52 (ddd, $J = 7.1, 5.5, 1.3$ Hz, 2H), 7.36 (d, $J = 6.1$ Hz, 1H), 7.09–7.03 (m, 1H).

3.4. X-ray Studies

Single crystals of $[RuT0B0(NO)](PF_6)_3$ (form A) were obtained by slow diffusion of dichloromethane into a concentrated solution of the compound (8–9 mg) in acetonitrile. Crystals of $[RuT1B0(DMSO)_{(S)}](PF_6)_3$ (form C) were obtained after extensive irradiation of $[RuT1B0(NO)](PF_6)_3$ (form A, 8 mg in 0.5 mL of DMSO), with a LED lamp at $\lambda = 395$ nm. After 6 h, the compound was found to be converted to form C at 94%, by 1H -NMR. The solvent was removed under vacuum with a Schlenk line. Slow diffusion of diethyl ether into a solution of the resulting solid dissolved in acetonitrile led to the formation of single crystals of form C.

Intensity data were collected at low temperature on an Apex2 Bruker diffractometer (equipped with a 30W air-cooled microfocuss Mo source ($\lambda = 0.71073$ Å)). The structures were solved using

SUPERFLIP [52] and refined by means of least-squares procedures using the programs of the PC version of CRYSTALS [53]. Atomic scattering factors were taken from the international tables for X-ray crystallography. All non-hydrogen atoms were refined anisotropically. The H atoms were located in a difference map, but those attached to carbon atoms were repositioned geometrically. The H atoms were refined with riding constraints. Absorption corrections were introduced using the program MULTISCAN [54]. The crystal structures have been deposited with the Cambridge Crystallographic Data Center (CCDC 1992867 for [RuT0B0(NO)](PF₆)₃, and CCDC 1992868 for [RuT1B0(DMSO_(S))](PF₆)₃).

3.5. Computational Studies

All the structures were optimized using density functional theory (DFT) with the standard hybrid B3LYP functional [55] complemented by the D3 version of Grimme's dispersion correction with Becke-Johnson damping [56]. A triple- ζ def2-TZVP basis set was used on all atoms and the corresponding pseudo-potential was used on the Ru center [57]. All the geometry optimizations were carried out within the polarizable continuum model (PCM) as implemented in Gaussian 09 [58] to describe the DMSO solvent. Calculations of vibrational harmonic frequencies were systematically performed in order to characterize the nature of the stationary points (minima or saddle points). UV-vis absorption spectra were simulated at the time-dependent DFT (TD-DFT) level using the same functional and same basis set as described above. The DMSO solvent was also described with PCM. The convoluted spectra were obtained using a Gaussian with a half-width at half-maximum of 1800 cm⁻¹ at each vertical transition given by TD-DFT. The chemical shifts were computed within the gauge including atomic orbital (GIAO) method [59–61]. These calculations were performed with B3LYP and PCM using an extended quadruple- ζ def2-QZVPP basis set on all atoms and the corresponding pseudo-potential for Ru [57]. Because of the presence of several conformers for some species (for example C was found to have four rotamers), the chemical shifts were computed as a weighted average of the chemical shifts for these various conformers using Boltzmann averaging.

4. Conclusions

[Ru(MeOPh-tpy)(bpy)(NO)](PF₆)₃ is an intriguing compound which undergoes a multi-step chemical and photochemical behavior in DMSO. By combining various experimental analyses (X-ray crystallography, ¹H-NMR, UV-vis absorption spectroscopy) and theoretical calculations, we were able to identify all the resulting products of these reactions. First, this complex exhibits an extreme sensitivity to trace of water leading to a reversible acid-base Ru-NO → RuNO₂ evolution stimulated by the intrinsic basic character of DMSO. Under irradiation, [Ru(MeOPh-tpy)(bpy)(NO)]³⁺ is subjected to a NO-release, with the concomitant generation of [Ru(MeOPh-tpy)(bpy)(DMSO_(S))]²⁺ as a photoproduct, in which the DMSO ligand is linked to the ruthenium by the sulfur atom. Under continued irradiation, the resulting Ru-DMSO complex undergoes a further, but reversible, isomerization process which leads to an equilibrium between the Ru-DMSO_(S) and Ru-DMSO_(O) species. By using different substituents attached to the tpy ligands, we were able to modulate the photoreactivity of this complex and of the photosubstitution product. In particular, by removing the electron-donor MeOPh group, the NO-photorelease is quenched to the profit of RuNO₂ formation. On the other hand, electron-withdrawing substituents favor the S→O linkage photo-isomerization of the Ru-DMSO_(S) photoproduct. Thus, our study brings further evidences of the very rich photochemistry of ruthenium nitrosyl complexes, with the most significant and positive feature that the presence of DMSO does not affect the capability of [Ru(tpy)(bpy)(NO)]³⁺ for the NO release (form A → form C + NO·), taking into account the frequent use of DMSO in practical biological test.

Supplementary Materials: The following are available online: Figures S1 and S2: NMR Spectra and assignments for forms A, B, C; Figure S3: NMR Spectra forms C/D; Figure S4: Computed structure; Figure S5: NMR tracking for the irradiation of [RuT1B0(NO)](PF₆)₃ in DMSO; Figure S6: Simulated electronic spectra for the Ru-DMSO_(S) and Ru-DMSO_(O) complexes.

Author Contributions: Conceptualization, P.G.L. and I.M.; Investigation, N.M., V.B., M.T., C.D. and M.B.-P.; Writing—Original draft preparation, N.M., P.G.L. and M.B.-P.; Writing—Review and editing, P.G.L., M.B.-P. and I.M.; Supervision, P.L., and I.M. All authors have read and agreed to the published version of the manuscript.

Funding: This research was funded by the Centre National de la Recherche Scientifique (CNRS) and the ANR-Photochromics (France).

Conflicts of Interest: The authors declare no conflict of interest.

References

1. Ignarro, L.; Freeman, B. *Nitric Oxide, Biology and Pathobiology*, 3rd ed.; Academic Press: Cambridge, MA, USA, 2017.
2. Xiang, H.J.; Guo, M.; Liu, J.G. Transition-Metal Nitrosyls for Photocontrolled Nitric Oxide Delivery. *Eur. J. Inorg. Chem.* **2017**, *2017*, 1586–1595. [[CrossRef](#)]
3. Mingos, D.M.P. *Nitrosyl Complexes in Inorganic Chemistry, Biochemistry and Medicine*; Springer: Berlin, Germany, 2014; Volume 154.
4. Fry, N.L.; Mascharak, P.K. Photoactive Ruthenium Nitrosyls as NO Donors: How to Sensitize Them toward Visible Light. *Acc. Chem. Res.* **2011**, *44*, 289–298. [[CrossRef](#)] [[PubMed](#)]
5. Rose, M.J.; Mascharak, P.K. Photoactive ruthenium nitrosyls: Effects of light and potential application as NO donors. *Coord. Chem. Rev.* **2008**, *252*, 2093–2114. [[CrossRef](#)] [[PubMed](#)]
6. Mikhailov, A.A.; Vorobyev, V.A.; Nadolinny, V.A.; Patrushev, Y.V.; Yudina, Y.S.; Kostin, G.A. Primary and secondary photochemical transformations of biologically active precursor-Nitro-Nitrosyl ruthenium complex. *J. Photochem. Photobiol. A Chem.* **2019**, *373*, 37–44. [[CrossRef](#)]
7. Orłowska, E.; Babak, M.V.; Doemoetoer, O.; Enyedy, E.A.; Rapta, P.; Zalibera, M.; Bucinsky, L.; Malcek, M.; Govind, C.; Karunakaran, V.; et al. NO Releasing and Anticancer Properties of Octahedral Ruthenium–Nitrosyl Complexes with Equatorial 1H-Indazole Ligands. *Inorg. Chem.* **2018**, *57*, 10702–10717. [[CrossRef](#)] [[PubMed](#)]
8. Crisalli, M.A.; Franco, L.P.; Silva, B.R.; Holanda, A.K.M.; Bendhack, L.M.; Da Silva, R.S.; Ford, P.C. Nitric oxide release from a photoactive water-soluble ruthenium nitrosyl. Biological effects. *J. Coord. Chem.* **2018**, *71*, 1690–1703. [[CrossRef](#)]
9. Kumar, R.; Kumar, S.; Bala, M.; Ratnam, A.; Singh, U.P.; Ghosh, K. Unprecedented oxidation of aldimine to carboxamido function during reactivity studies on ruthenium complex with acidified nitrite solution: Synthesis of ruthenium nitrosyl complex having {RuNO}⁶ moiety and photorelease of coordinated NO. *J. Organomet. Chem.* **2018**, *863*, 77–83. [[CrossRef](#)]
10. Guo, M.; Xiang, H.J.; Wang, Y.; Zhang, Q.L.; An, L.; Yang, S.P.; Ma, Y.; Wang, Y.; Liu, J.G. Ruthenium nitrosyl functionalized graphene quantum dots as an efficient nanoplatfrom for NIR-light-controlled and mitochondria-targeted delivery of nitric oxide combined with photothermal therapy. *Chem. Commun.* **2017**, *53*, 3253–3256. [[CrossRef](#)]
11. Rodrigues, G.L.S.; Rocha, W.R. Formation and Release of NO from Ruthenium Nitrosyl Ammine Complexes [Ru(NH₃)₅(NO)]^{2+/3+} in Aqueous Solution: A Theoretical Investigation. *J. Phys. Chem. B* **2016**, *120*, 11821–11833. [[CrossRef](#)]
12. Cacita, N.; Possato, B.; da Silva, C.F.N.; Paulo, C.M.; Formiga, A.L.B.; Bendhack, L.M.; Nikolaou, S. Investigation of a novel trinuclear μ-oxo ruthenium complex as a potential nitric oxide releaser for biological purposes. *Inorg. Chim. Acta.* **2015**, *429*, 114–121. [[CrossRef](#)]
13. Pereira, J.C.M.; Souza, M.L.; Franco, D.W. Nitric Oxide and Nitroxyl Products from the Reaction of L-Cysteine with trans-[RuNO(NH₃)₄P(OEt)₃](PF₆)₃. *Eur. J. Inorg. Chem.* **2015**, *2015*, 1005–1011. [[CrossRef](#)]
14. Reynolds, W.R. Dimethyl Sulfoxide in Inorganic Chemistry. In *Progress in Inorganic Chemistry*; Lippard, S.J., Ed.; Interscience: New York, NY, USA, 1970; Volume 12.
15. Cordones, A.A.; Lee, J.H.; Hong, K.; Cho, H.; Garg, K.; Boggio-Pasqua, M.; Rack, J.J.; Huse, N.; Schoenlein, R.W.; Kim, T.K. Transient metal-centered states mediate isomerization of a photochromic ruthenium-sulfoxide complex. *Nat. Commun.* **2018**, *9*, 1989. [[CrossRef](#)] [[PubMed](#)]
16. Rack, J.J.; Mockus, N.V. Room-Temperature Photochromism in cis- and trans-[Ru(bpy)₂(dmsO)₂]²⁺. *Inorg. Chem.* **2003**, *42*, 5792–5794. [[CrossRef](#)] [[PubMed](#)]

17. Rachford, A.A.; Rack, J.J. Picosecond isomerization in photochromic ruthenium–dimethyl sulfoxide complexes. *J. Am. Chem. Soc.* **2006**, *128*, 14318–14324. [[CrossRef](#)]
18. Göttle, A.J.; Dixon, I.M.; Alary, F.; Heully, J.-L.; Boggio-Pasqua, M. Adiabatic versus nonadiabatic photoisomerization in photochromic ruthenium sulfoxide complexes: A mechanistic picture from density functional theory calculations. *J. Am. Chem. Soc.* **2011**, *133*, 9172–9174. [[CrossRef](#)]
19. Ciofini, I.; Daul, C.; Adamo, C. Phototriggered linkage isomerization in ruthenium–dimethylsulfoxide complexes: Insights from theory. *J. Phys. Chem. A* **2003**, *107*, 11182–11190. [[CrossRef](#)]
20. McClure, B.A.; Rack, J.J. Isomerization in photochromic ruthenium sulfoxide complexes. *Eur. J. Inorg. Chem.* **2010**, *2010*, 3895–3904. [[CrossRef](#)]
21. Pawlicki, M.; Collins, H.A.; Denning, R.G.; Anderson, H.L. Two-photon absorption and the design of two-photon dyes. *Angew. Chem. Int. Ed.* **2009**, *48*, 3244–3266. [[CrossRef](#)]
22. Strehmel, B.; Strehmel, V. Two-photon physical organic, and polymer chemistry: Theory, techniques, chromophore design, and applications. *Adv. Photochem.* **2007**, *29*, 111–341. [[CrossRef](#)]
23. Bukhanko, V.; Lacroix, P.G.; Sasaki, I.; Tassé, M.; Mallet-Ladeira, S.; Voitenko, Z.; Malfant, I. Mechanism and oxidation state involved in the nitric oxide (NO) photorelease in a terpyridine-bipyridine-based ruthenium nitrosyl complex. *Inorg. Chim. Acta* **2018**, *482*, 195–205. [[CrossRef](#)]
24. Roose, M.; Tassé, M.; Lacroix, P.G.; Malfant, I. Nitric oxide (NO) photo-release in a series of ruthenium–nitrosyl complexes: New experimental insights in the search for a comprehensive mechanism. *New J. Chem.* **2019**, *43*, 755–767. [[CrossRef](#)]
25. Garcia, J.S.; Alary, F.; Boggio-Pasqua, M.; Dixon, I.M.; Heully, J.-L. Is photoisomerization required for NO photorelease in ruthenium nitrosyl complexes? *J. Mol. Model.* **2016**, *22*, 1–10. [[CrossRef](#)] [[PubMed](#)]
26. García, J.S.; Alary, F.; Boggio-Pasqua, M.; Dixon, I.M.; Malfant, I.; Heully, J.-L. Establishing the Two-Photon Linkage Isomerization Mechanism in the Nitrosyl Complex $\text{trans}[\text{RuCl}(\text{NO})(\text{py})_4]^{2+}$ by DFT and TDDFT. *Inorg. Chem.* **2015**, *54*, 8310–8318. [[CrossRef](#)] [[PubMed](#)]
27. Tfouni, E.; Krieger, M.; McGarvey, B.R.; Franco, D.W. Structure, chemical and photochemical reactivity and biological activity of some ruthenium amine nitrosyl complexes. *Coord. Chem. Rev.* **2003**, *236*, 57–69. [[CrossRef](#)]
28. Cormary, B.; Malfant, I.; Buron-Le Cointre, M.; Toupet, L.; Delley, B.; Schaniel, D.; Morckus, N.; Woike, T.; Fejfarova, K.; Petricek, V.; et al. $[\text{Ru}(\text{py})_4\text{ClNO}](\text{PF}_6)_2 \cdot 0.5 \text{H}_2\text{O}$: A model system for structural determination and ab initio calculations of photo-induced linkage NO isomers. *Acta Crystallogr. Sect. B* **2009**, *65*, 612–623. [[CrossRef](#)] [[PubMed](#)]
29. Schaniel, D.; Cormary, B.; Malfant, I.; Valade, L.; Woike, T.; Delley, B.; Kraemer, K.W.; Guedel, H.U. Photogeneration of two metastable NO linkage isomers with high populations of up to 76% in $\text{trans}[\text{RuCl}(\text{py})_4(\text{NO})](\text{PF}_6)_2 \cdot \frac{1}{2} \text{H}_2\text{O}$. *Phys. Chem. Chem. Phys.* **2007**, *9*, 3717–3724. [[CrossRef](#)]
30. Mikhailov, A.A.; Wenger, E.; Kostin, G.A.; Schaniel, D. Room-Temperature Photogeneration of Nitrosyl Linkage Isomers in Ruthenium Nitrosyl Complexes. *Chem. Eur. J.* **2019**, *25*, 7569–7574. [[CrossRef](#)]
31. Karidi, K.; Garoufis, A.; Hadjiliadis, N.; Lutz, M.; Spek, L.; Reedijk, J. Synthesis, Characterization, and DNA-Binding Studies of Nitro(oligopyridine)ruthenium(II) Complexes. *Inorg. Chem.* **2006**, *45*, 10282–10292. [[CrossRef](#)]
32. Xiang, J.C.; Gao, Q.H.; Wu, A.X. *Solvents as Reagents in Organic Synthesis: Reactions and Applications*; Wiley-VCH, Wiley: Hoboken, NJ, USA, 2017; pp. 315–353.
33. Liang, Y.F.; Wu, K.; Song, S.; Li, X.; Huang, X.; Jiao, N. I₂- or NBS-Catalyzed Highly Efficient α -Hydroxylation of Ketones with Dimethyl Sulfoxide. *Org. Lett.* **2015**, *17*, 876–8792. [[CrossRef](#)]
34. Cao, Z.; Lv, H.; Liu, Y.; Nie, Z.; Liu, H.; Yang, T.; Luo, W.; Liu, Q.; Guo, C. Dimethyl Sulfoxide Oxygen Donor-Based Annulation of Ketones and Ammonium Persulfate: Regioselective Synthesis of 2, 4-disubstituted Oxazoles. *Adv. Synth. Catal.* **2019**, *361*, 1632–1640. [[CrossRef](#)]
35. Zhang, X.; Li, S.S.; Wang, L.; Xu, L.; Xiao, J.; Liu, Z.J. 2-Methylquinoline promoted oxidative ring-opening of N-sulfonyl aziridines with DMSO: Facile synthesis of α -amino aryl ketones. *Tetrahedron* **2016**, *72*, 8073–8077. [[CrossRef](#)]
36. Sultana, F.; Shaik, S.P.; Alarifi, A.; Srivastava, A.K.; Kamal, A. Transition-Metal-Free Oxidative Cross-Coupling of Methylarenes with Imidazoheterocycles towards Efficient C(sp²)–H Carbonylation. *Asian J. Org. Chem.* **2017**, *6*, 890–897. [[CrossRef](#)]

37. Enemark, J.H.; Feltham, R.R. Principles of structure, bonding, and reactivity for metal nitrosyl complexes. *Coord. Chem. Rev.* **1974**, *13*, 339–406.
38. Ogasawara, M.; Huang, D.; Streib, W.E.; Huffman, J.C.; Gallego-Planas, N.; Maseras, F.; Eisenstein, O.; Caulton, K.G. RuX(CO)(NO)L₂ and Ru(CO)(NO)L²⁺: Ru(0) or Ru(II) or In Between? *J. Am. Chem. Soc.* **1997**, *119*, 8642–8651. [[CrossRef](#)]
39. Rack, J.J.; Winkler, J.R.; Gray, H.B. Phototriggered Ru(II)-dimethylsulfoxide linkage isomerization in crystals and films. *J. Am. Chem. Soc.* **2001**, *123*, 2432–2433. [[CrossRef](#)] [[PubMed](#)]
40. Enriquez-Cabrera, A.; Sasaki, I.; Bukhanko, V.; Tassé, M.; Mallet-Ladeira, S.; Lacroix, P.G.; Barba-Barba, R.M.; Ramos-Ortiz, G.; Farfan, N.; Voitenko, Z.; et al. Replacing Two Chlorido Ligands by a Bipyridine Ligand in Ruthenium Nitrosyl Complexes with NO-Release Capabilities: A Comparative Study. *Eur. J. Inorg. Chem.* **2017**, 1446–1456. [[CrossRef](#)]
41. Enriquez-Cabrera, A.; Lacroix, P.G.; Sasaki, I.; Mallet-Ladeira, S.; Farfan, N.; Barba-Barba, R.M.; Ramos-Ortiz, G.; Malfant, I. Comparison of Carbazole and Fluorene Donating Effects on the Two-Photon Absorption and Nitric Oxide Photorelease Capabilities of a Ruthenium–Nitrosyl Complex. *Eur. J. Inorg. Chem.* **2018**, *2018*, 531–543. [[CrossRef](#)]
42. King, A.W.; Wang, L.; Rack, J.J. Excited state dynamics and isomerization in ruthenium sulfoxide complexes. *Acc. Chem. Res.* **2015**, *48*, 1115–1122. [[CrossRef](#)]
43. Rack, J.J. Electron transfer triggered sulfoxide isomerization in ruthenium and osmium complexes. *Coord. Chem. Rev.* **2009**, *253*, 78–85. [[CrossRef](#)]
44. Roeker, L.; Dobson, J.C.; Vining, W.J.; Meyer, T.J. Oxygen atom transfer in the oxidations of dimethyl sulfide and dimethyl sulfoxide by bis(bipyridine)oxo(pyridine)ruthenium(2+). *Inorg. Chem.* **1987**, *26*, 779–781. [[CrossRef](#)]
45. Root, M.J.; Deutsch, E. Synthesis and characterization of (bipyridine)(terpyridine)(chalcogenoether) ruthenium (II) complexes. Kinetics and mechanism of the hydrogen peroxide oxidation of [(bpy)(tpy)RuS(CH₃)₂]²⁺ to [(bpy)(tpy)RuS(O)(CH₃)₂]²⁺. Kinetics of the aquation of [(bpy)(tpy)RuS(O)(CH₃)₂]²⁺. *Inorg. Chem.* **1985**, *24*, 1464–1471.
46. Göttle, A.J.; Alary, F.; Dixon, I.M.; Heully, J.-L.; Boggio-Pasqua, M. Unravelling the S → O Linkage Photoisomerization Mechanisms in cis- and trans-[Ru(bpy)₂(DMSO)₂]²⁺ Using Density Functional Theory. *Inorg. Chem.* **2014**, *53*, 6752–6760. [[CrossRef](#)] [[PubMed](#)]
47. Murphy, W.R., Jr.; Takeuchi, K.; Barley, M.H.; Meyer, T.J. Mechanism of reduction of bound nitrite to ammonia. *Inorg. Chem.* **1986**, *25*, 1041–1053. [[CrossRef](#)]
48. Pipes, D.W.; Meyer, T.J. Comparisons between polypyridyl nitrosyl complexes of osmium (II) and ruthenium (II). *Inorg. Chem.* **1984**, *23*, 2466–2472. [[CrossRef](#)]
49. Patel, M.N.; Joshi, H.N.; Patel, C.R. Interactions with herring sperm DNA and biological studies of sparfloxacin drug-based copper (II) compounds. *Appl. Organometal. Chem.* **2012**, *26*, 641–649. [[CrossRef](#)]
50. Koohmareh, G.A.; Sharifi, M. Synthesis, characterization, and coordination behavior of copoly(styrene-maleimide) functionalized with terpyridine. *J. Appl. Polym. Sci.* **2010**, *116*, 179–183. [[CrossRef](#)]
51. Takeuchi, K.J.; Thompson, M.S.; Pipes, D.W.; Meyer, T.J. Redox and spectral properties of monooxo polypyridyl complexes of ruthenium and osmium in aqueous media. *Inorg. Chem.* **1984**, *23*, 1845–1851. [[CrossRef](#)]
52. Palatinus, L.; Chapuis, G. SUPERFLIP—a computer program for the solution of crystal structures by charge flipping in arbitrary dimensions. *J. Appl. Cryst.* **2007**, *40*, 786–790. [[CrossRef](#)]
53. Betteridge, P.W.; Carruthers, J.R.; Cooper, R.I.; Prout, K.; Watkin, D.J. CRYSTALS version 12: Software for guided crystal structure analysis. *J. Appl. Cryst.* **2003**, *36*, 1487. [[CrossRef](#)]
54. Blessing, R.H. Blessing R.H. An empirical correction for absorption anisotropy. *Acta Crystallogr. Sect. A* **1995**, *51*, 33–38. [[CrossRef](#)]
55. Becke, A.D. Density-functional thermochemistry. III. The role of exact exchange. *J. Chem. Phys.* **1993**, *98*, 5648–5652. [[CrossRef](#)]
56. Grimme, S.; Ehrlich, S.; Goerigk, L. Effect of the damping function in dispersion corrected density functional theory. *J. Comp. Chem.* **2011**, *32*, 1456–1465. [[CrossRef](#)] [[PubMed](#)]
57. Weigend, F.; Ahlrichs, R. Balanced basis sets of split valence, triple zeta valence and quadruple zeta valence quality for H to Rn: Design and assessment of accuracy. *Phys. Chem. Chem. Phys.* **2005**, *7*, 3297–3305. [[CrossRef](#)] [[PubMed](#)]

58. Frisch, M.J.; Trucks, G.W.; Schlegel, H.B.; Scuseria, G.E.; Robb, M.A.; Cheeseman, J.R.; Scalmani, G.; Barone, V.; Mennucci, B.; Petersson, G.A.; et al. *Gaussian 09*; Revision D.01; Gaussian, Inc.: Wallingford, CT, USA, 2009.
59. London, F. The quantic theory of inter-atomic currents in aromatic combinations. *J. Phys. Radium* **1937**, *8*, 397–409. [[CrossRef](#)]
60. Ditchfield, R. Self-consistent perturbation theory of diamagnetism. 1. Gauge-invariant LCAO method for N.M.R. chemical shifts. *Mol. Phys.* **1974**, *27*, 789–807. [[CrossRef](#)]
61. Wolinski, K.; Hinton, J.F.; Pulay, P. Efficient Implementation of the Gauge-Independent Atomic Orbital Method for NMR Chemical Shift Calculations. *J. Am. Chem. Soc.* **1990**, *112*, 8251–8260. [[CrossRef](#)]

Sample Availability: Samples of the compounds are not available from the authors.



© 2020 by the authors. Licensee MDPI, Basel, Switzerland. This article is an open access article distributed under the terms and conditions of the Creative Commons Attribution (CC BY) license (<http://creativecommons.org/licenses/by/4.0/>).